# Implementation of Free-Surface Condition for Finite-Difference Time-Domain Method Using a Staggered Grid with the Collocated Grid Points of Velocities

Takashi Yasui*[,1], Koji Hasegawa[2], and Koichi Hirayama[1]

[1]*Kitami Institute of Technology, Kitami, Hokkaido 090-8507, Japan*
[2]*Muroran Institute of Technology, Muroran, Hokkaido 050-8585, Japan*

The finite-difference time-domain (FD-TD) method using a staggered grid with the collocated grid points of velocities (SGCV) in two dimensions was applied to Lamé mode resonators on an isotropic solid. Their resonance frequencies of the fundamental Lamé mode were examined to confirm the validity of the SGCV models of the free surfaces. The resonance frequency obtained with an SGCV, which uses bipolynomial interpolation with values of velocity on six adjoining grids to evaluate the derivatives of velocity vector fields on a grid, showed good agreement with the analytical resonance frequency.

## 1. Introduction

The finite-difference time-domain (FD-TD) method is a powerful and attractive tool for modeling the propagation and scattering of elastic waves in solids. Discretization of two first-order partial differential equations with finite-difference approximations results in a staggered grid (SG),[1,2] a rotated staggered grid,[3,4] a diagonally staggered grid,[5–7] or a Levedev grid.[8–10]

For an isotropic solid in seismology, a staggered grid for velocity and stress models, which use schemes of second-order accuracy in the time difference and second- or fourth-order accuracy in the spatial difference [(2,2) and (2,4) schemes, respectively] has been reported.[1,2] To readers who are unfamiliar with the FD-TD method, we recommend the book of Moczo et al.[11] The central difference approximation of time derivatives results in a primary grid of stresses and an auxiliary grid of velocities that are staggered by half the time interval $\Delta_t/2$. In addition, the nodes of the $x$-, $y$-, and $z$-components of velocities are staggered by half the spatial size of a uniform unit cell along the $x$-, $y$-, and $z$-axes, respectively, because of the finite-difference approximation of the relation between strains and the partial derivatives of particle velocities. These arrangements

*E-mail: yasui@mail.kitami-it.ac.jp

of the grid points show that control volumes corresponding to the law of momentum conservation are interleaved for the $x$-, $y$-, and $z$-components from the perspective of the finite integration technique (FIT).[12–17)]

For anisotropic solids, rotated staggered,[3,4)] diagonally staggered,[5–7)] and Levedev grids[8–10)] have been developed. In the rotated and diagonally staggered grids, interpolations of velocity vectors and stress components are used to approximate velocity gradients and stress divergences. In the Levedev grids, no interpolation is used but the number of points of velocities and stresses included in the unit cell is more than in the rotated and the diagonally staggered grids.

Recently, we presented a staggered grid using the collocated grid points of velocities (SGCV) for modeling the propagation of elastic waves in anisotropic solids by the FD-TD method.[18)] For the simple imposition of boundary conditions on FD-TD models, the new grid was derived from a single control volume of the momentum conservation law and line integrations of the displacement gradient. Abandoning the cross-shape arrangement of the velocity vector results in interpolations of the velocity components away from grid points. Numerical dispersions of vertically polarized shear waves (SV-waves) and longitudinal waves (P-waves) in an infinite isotropic solid by the (2,2) and (2,4) schemes have been investigated, and it has been reported[18)] that the interpolation with third-degree bipolynomials gives comparable results to the staggered grids.[1,2)]

To model elastic wave devices by the FD-TD method, boundary conditions on planar free surfaces should be examined. With the conventional staggered grids,[1,2)] as shown in Fig. 1, FD-TD models can use the stress-imaging technique,[2)] the vacuum formalism,[3)] or the adjusted staggered scheme.[4,19)] Because the velocity vectors are at the center grid points and all stresses on the grid surfaces are normal components in the FD-TD models using the SGCV, as shown in Fig. 2, the imposition of planar free-surface conditions involves setting all stress components on the surface equal to zero. However, interpolations of the velocity vectors away from the grid points near the free surface are required to compute velocity gradients. Hence, a modification must be introduced. Extrapolation techniques or one-sided finite differentiation schemes are candidates for the immediate computation of the velocity gradients at the grid points of stresses.

In this paper, for the computation of velocity gradients, we examined the derivatives of interpolation polynomials of velocity vector fields for the FD-TD models using the SGCV in two dimensions. We extract the resonance frequency of the fundamental Lamé mode of a resonator on an isotropic solid and confirm the validity of the SGCV models

of the free surfaces.

## 2. Modeling Planar Free Surfaces by FD-TD using the SGCV in Two Dimensions

### 2.1 Time update equations based on FD-TD scheme

In an isotropic solid in two dimensions, the cell of a uniform SGCV for SV- and P-wave propagation reduces to the grid shown in Fig. 2. Here, $\Delta$ is the spatial interval of the grid, $I$ and $J$ are integers for a grid point with the position vector $\boldsymbol{p} = (I\hat{x} + J\hat{y})\Delta$, where $\hat{x}$ and $\hat{y}$ are the unit vectors in the $x$- and $y$-directions, and $v_i$ and $T_{ij}$ $(i, j = x, y)$ are the $i$-component of a particle velocity and the $ij$-component of a stress tensor, respectively.

Newton's equation of motion and the relations between displacement gradient tensors $\Gamma_{ij}$ and velocity vectors are modeled by FD-TD schemes in two dimensions as follows:

$$\rho\frac{v_i^{K+1/2}(I,J) - v_i^{K-1/2}(I,J)}{\Delta_t} = \frac{T_{ix}^K(I+\frac{1}{2},J) - T_{ix}^K(I-\frac{1}{2},J)}{\Delta} + \frac{T_{iy}^K(I,J+\frac{1}{2}) - T_{iy}^K(I,J-\frac{1}{2})}{\Delta}, \quad (1)$$

$$\left.\frac{\partial\Gamma_{ix}}{\partial t}\right|_{(I-1/2,J)}^{K+1/2} = \frac{v_i^{K+1/2}(I,J) - v_i^{K+1/2}(I-1,J)}{\Delta}, \quad (2)$$

$$\left.\frac{\partial\Gamma_{iy}}{\partial t}\right|_{(I,J-1/2)}^{K+1/2} = \frac{v_i^{K+1/2}(I,J) - v_i^{K+1/2}(I,J-1)}{\Delta} \quad (3)$$

for $i = x, y$. Here, $\rho$ is the mass density, $t = K\Delta_t$ is the time, where $K$ is an integer and $\Delta_t$ is the time interval, and $f^K(I,J)$ and $\left.\frac{\partial f}{\partial t}\right|_{(I,J)}^K$ denote the values at the space grid $(x,y) = (I\Delta, J\Delta)$ and the time point $t = K\Delta_t$ for a scalar function of space and time $f(x,y,t)$ and its time derivative, respectively. Using the derivative of the stress and strain relation with respect to time and Eqs. (2) and (3), we obtain the following relations:

$$\frac{T_{xx}^K(I-\frac{1}{2},J) - T_{xx}^{K-1}(I-\frac{1}{2},J)}{\Delta_t} = (\lambda+2\mu)\frac{v_x^{K+1/2}(I,J) - v_x^{K+1/2}(I-1,J)}{\Delta} + \lambda\left.\frac{\partial\tilde{v}_y}{\partial y}\right|_{(I-1/2,J)}^{K+1/2}, \quad (4)$$

$$\frac{T_{yx}^{K}(I-\frac{1}{2},J)-T_{yx}^{K-1}(I-\frac{1}{2},J)}{\Delta_t} = \mu\frac{v_y^{K+1/2}(I,J)-v_y^{K+1/2}(I-1,J)}{\Delta}+\mu\left.\frac{\partial\tilde{v}_x}{\partial y}\right|_{(I-1/2,J)}^{K+1/2}, \quad (5)$$

$$\frac{T_{xy}^{K}(I,J-\frac{1}{2})-T_{xy}^{K-1}(I,J-\frac{1}{2})}{\Delta_t} = \mu\frac{v_x^{K+1/2}(I,J)-v_x^{K+1/2}(I,J-1)}{\Delta}+\mu\left.\frac{\partial\tilde{v}_y}{\partial x}\right|_{(I,J-1/2)}^{K+1/2}, \quad (6)$$

$$\frac{T_{yy}^{K}(I,J-\frac{1}{2})-T_{yy}^{K-1}(I,J-\frac{1}{2})}{\Delta_t} = (\lambda+2\mu)\frac{v_y^{K+1/2}(I,J)-v_y^{K+1/2}(I,J-1)}{\Delta}+\lambda\left.\frac{\partial\tilde{v}_x}{\partial x}\right|_{(I,J-1/2)}^{K+1/2}. \quad (7)$$

Here $\lambda$ and $\mu$ are the Lamé constants, and $\tilde{v}_i^K(I,J)$ and $\left.\frac{\partial\tilde{v}_i}{\partial j}\right|_{(I,J)}^{K}$ $(i,j=x,y)$ denote the velocity $v_i(I\Delta,J\Delta,K\Delta_t)$ and its gradient at the space grid $(x,y)=(I\Delta,J\Delta)$ and the time point $t=K\Delta_t$, respectively. These values are computed by the interpolation schemes described below because the velocity components on the corners of the SGCV grids are required in the standard FD-TD scheme.

To compute the velocity gradients $\partial\tilde{v}_i/\partial j|_{(I,J)}^{K}$ $(i,j=x,y)$ in Eqs. (4)–(7), first the velocity components on the corner points of the SGCV are interpolated as

$$\tilde{v}_i^{K+1/2}(I-\frac{1}{2},J-\frac{1}{2}) = \frac{1}{4}\Big(v_i^{K+1/2}(I,J)+v_i^{K+1/2}(I-1,J) +v_i^{K+1/2}(I,J-1)+v_i^{K+1/2}(I-1,J-1)\Big), \quad (8)$$

$$\tilde{v}_i^{K+1/2}(I+\frac{1}{2},J-\frac{1}{2}) = \frac{1}{4}\Big(v_i^{K+1/2}(I,J)+v_i^{K+1/2}(I+1,J) +v_i^{K+1/2}(I,J-1)+v_i^{K+1/2}(I+1,J-1)\Big), \quad (9)$$

$$\tilde{v}_i^{K+1/2}(I-\frac{1}{2},J+\frac{1}{2}) = \frac{1}{4}\Big(v_i^{K+1/2}(I,J)+v_i^{K+1/2}(I-1,J) +v_i^{K+1/2}(I,J+1)+v_i^{K+1/2}(I-1,J+1)\Big), \quad (10)$$

$$\tilde{v}_i^{K+1/2}(I+\frac{1}{2},J+\frac{1}{2}) = \frac{1}{4}\Big(v_i^{K+1/2}(I,J)+v_i^{K+1/2}(I+1,J) +v_i^{K+1/2}(I,J+1)+v_i^{K+1/2}(I+1,J+1)\Big) \quad (11)$$

for $i = x, y$, then the velocity gradients are computed as follows:[18)]

$$\begin{aligned}\left.\frac{\partial \tilde{v}_i}{\partial x}\right|_{(I,J-1/2)}^{K+1/2} =& \frac{\tilde{v}_i^{K+1/2}(I+\frac{1}{2}, J-\frac{1}{2}) - \tilde{v}_i^{K+1/2}(I-\frac{1}{2}, J-\frac{1}{2})}{\Delta} \\ =& \frac{1}{4\Delta}\Big(v_i^{K+1/2}(I+1, J) + v_i^{K+1/2}(I+1, J-1) \\ & - v_i^{K+1/2}(I-1, J) - v_i^{K+1/2}(I-1, J-1)\Big), \end{aligned} \tag{12}$$

$$\begin{aligned}\left.\frac{\partial \tilde{v}_i}{\partial y}\right|_{(I-1/2,J)}^{K+1/2} =& \frac{\tilde{v}_i^{K+1/2}(I-\frac{1}{2}, J+\frac{1}{2}) - \tilde{v}_i^{K+1/2}(I-\frac{1}{2}, J-\frac{1}{2})}{\Delta} \\ =& \frac{1}{4\Delta}\Big(v_i^{K+1/2}(I, J+1) + v_i^{K+1/2}(I-1, J+1) \\ & - v_i^{K+1/2}(I, J-1) - v_i^{K+1/2}(I-1, J-1)\Big) \end{aligned} \tag{13}$$

for $i = x, y$.

## 2.2 FD-TD model of free surfaces using SGCV

In this subsection, we represent a function of space and time $f(x, y, t)$ and its gradient at the position $\boldsymbol{r} = x\hat{x} + y\hat{y}$ and time $t$ as $f(\boldsymbol{r})$ and $\partial f/\partial j|_{\boldsymbol{r}}$ $(j = x, y)$, respectively. Here, the time $t$ is omitted to simplify the discussion. Consider SGCV grids on free surfaces normal to the $x$-axis as shown in Figs. 3(a) and 3(b). Here, $\boldsymbol{p}_n$ $(n = 1, \ldots, 6)$ denote the position vectors of the grid points for the velocity components, and $\boldsymbol{r}_n = x_n\hat{x} + y_n\hat{y}$ $(n = 1, 2)$ denote the grid points for $T_{xy}$ and $T_{yy}$ located just inside the free surfaces on the left and right, respectively. At the grid points $\boldsymbol{r}_n$ $(n = 1, 2)$, the velocity gradients $\partial \tilde{v}_i/\partial x|_{\boldsymbol{r}_n}$ $(i = x, y)$ cannot be computed with Eqs. (8)–(13) because of the lack of grid points of the velocity vector in the vacuum.

Recalling that the derivative of an interpolation polynomial is a scheme for numerical differentiation, we can compute the required gradients $\partial \tilde{v}_i/\partial x|_{\boldsymbol{r}_n}$ $(n = 1, 2)$ immediately: when a tensor product of two polynomial interpolations of the $i$-component of the velocity vector on adjoining grids,

$$v_i(\boldsymbol{r}) = \sum_{l=0}^{D_x-1}\sum_{m=0}^{D_y-1} C_{lm}(x - x_n)^l(y - y_n)^m \tag{14}$$

for $i = x, y$ and $n = 1, 2$, is used, we obtain $\frac{\partial \tilde{v}_i}{\partial x}\big|_{\boldsymbol{r}_n} = C_{10}$. Here, $D_x$ and $D_y$ denote the interpolation orders in the $x$- and $y$-directions, respectively, and the coefficient $C_{10}$ is computed using the velocities on $D_x \times D_y$ adjoining grids.

From Eq. (14), we obtain the following:

$$\left.\frac{\partial \tilde{v}_i}{\partial x}\right|_{\boldsymbol{r}_1} = \frac{1}{2\Delta}\left[v_i(\boldsymbol{p}_2) - v_i(\boldsymbol{p}_3) - v_i(\boldsymbol{p}_4) + v_i(\boldsymbol{p}_5)\right], \tag{15}$$

$$\left.\frac{\partial \tilde{v}_i}{\partial x}\right|_{\boldsymbol{r}_2} = \frac{1}{2\Delta}\left[v_i(\boldsymbol{p}_1) - v_i(\boldsymbol{p}_2) - v_i(\boldsymbol{p}_5) + v_i(\boldsymbol{p}_6)\right] \tag{16}$$

with four adjoining grids ($D_x = 2$, $D_y = 2$) and

$$\left.\frac{\partial \tilde{v}_i}{\partial x}\right|_{\boldsymbol{r}_1} = \frac{-1}{4\Delta}\left\{[v_i(\boldsymbol{p}_1) + v_i(\boldsymbol{p}_6)] - 4[v_i(\boldsymbol{p}_2) + v_i(\boldsymbol{p}_5)] + 3[v_i(\boldsymbol{p}_3) + v_i(\boldsymbol{p}_4)]\right\}, \tag{17}$$

$$\left.\frac{\partial \tilde{v}_i}{\partial x}\right|_{\boldsymbol{r}_2} = \frac{1}{4\Delta}\left\{3[v_i(\boldsymbol{p}_1) + v_i(\boldsymbol{p}_6)] - 4[v_i(\boldsymbol{p}_2) + v_i(\boldsymbol{p}_5)] + [v_i(\boldsymbol{p}_3) + v_i(\boldsymbol{p}_4)]\right\} \tag{18}$$

with six adjoining grids ($D_x = 3$, $D_y = 2$).

For free surfaces normal to the $y$-axis, we obtain the velocity gradient $\partial \tilde{v}_i/\partial y|_{\boldsymbol{r}_n} = C_{01}$ $(n = 1, 2)$ from Eq. (14), from which similar formulae to Eqs. (15)–(18) are derived.

## 3. Analysis of a Lamé Mode Resonator

### 3.1 FD-TD models

In two dimensions, we consider a Lamé mode resonator that is a square with a side length of $L$ on an isotropic solid with Poisson's ratio 0.25 as shown in Fig. 4. When the wavelength of the SV-wave at the frequency $f_s$ is $2L$, the fundamental resonance frequency $f_1$ of the Lamé mode is $f_1 = \sqrt{2} f_s$. In the following results, $f_1 = 1$ MHz and $R = v_p \Delta_t/\Delta = 0.5$, the latter is chosen to ensure numerical stability and computational efficiency. Here, $v_p$ is the phase velocity of the P-wave in the solid. At the grid points for $T_{ij}$ $(i, j = x, y)$ located just inside the free surfaces, we choose four or six adjoining grids for the computation of $\partial \tilde{v}_i/\partial j$ $(i, j = x, y)$.

### 3.2 Computation of the resonance frequency

The observation point and vibration point are $(L/4, L/4)$ and $(-L/4, -L/4)$, respectively, on the $x$-$y$ plane with the origin on the center of the square resonator as shown in Fig. 4. The vibration of the $x$-component of the particle velocity is expressed as a sine-modulated Gaussian pulse with center frequency $f_1$ and a full width at half maximum in time of $83.26RL/v_p$, which gives a broad enough spectral bandwidth to extract the resonance frequency. The resulting discrete time response of the particle velocity of the observation point is shown in Fig. 5. Applying the discrete Fourier transform to the time response at the observation point in the interval from $N_s\Delta_t$ to $N_e\Delta_t$, we extract the

resonance frequency of the resonator. Here, $N_s$ and $N_e$ are the numbers of time steps corresponding to the start and end sampling times, respectively. Figure 6 shows the power spectrum with $L/\Delta = 2^6$, $N_s\Delta_t = 2^8 RLv_p \approx 52.25$ $\mu$s, $N_e\Delta_t = 2^{10}RL/v_p$, and the coefficients $C_{10}$ and $C_{01}$, computed using six adjoining grids. Figures 7(a) and 7(b) respectively show the distributions of the $x$- and $y$-components of the particle velocity at the end of the computation ($t = N_e\Delta_t$). These results are in good agreement with the exact solutions given as $v_x(x, y, t) = \mathrm{Re}[-\sin(\beta x)\cos(\beta y)e^{j\omega t}]$ and $v_y(x, y, t) = \mathrm{Re}[\cos(\beta x)\sin(\beta y)e^{j\omega t}]$, where $\beta = \pi/L$ for the fundamental Lamé mode, and $j$ and $\omega$ are the imaginary unit and angular frequency, respectively. The extracted resonance frequency is 0.9999 MHz and we can thus confirm the validity of our free surface models.

Figure 8 shows extracted resonance frequencies with $N_s\Delta_t = 2^8 RL/v_p \approx 52.25$ $\mu$s and $N_e\Delta_t = 2^N RL/v_p$, where $2^N$ is the total numbers of steps and $N$ is an integer. The computed results using four and six adjoining grids with $L/\Delta = 4$ are 0.992 and 0.985 MHz, respectively, and we expect that the use of six adjoining grids will be preferable to obtain an accurate model. We can observe good convergence with $L/\Delta = 2^6$ ($\circ$ and $\square$ on dashed lines in Fig. 8).

## 4. Conclusions

In this paper, we examined the derivatives of interpolation polynomials of velocity vector fields for FD-TD models using the SGCV in two dimensions. We extracted the resonance frequency of the fundamental Lamé mode of a resonator on an isotropic solid. To compute the velocity gradients on the edges of the resonator, we used polynomial interpolations of the velocity vector on adjoining grids. We found that the use of six adjoining grids was preferable to obtain an accurate model.

## References


1) J. Virieux: Geophysics **51** (1986) 889.
2) A. Levander: Geophysics **53** (1988) 1425.
3) E. H. Saenger, N. Gold, and S. A. Shapiro: Wave Motion **31** (2000) 77.
4) T. Bohlen and E. H. Saenger: Geophysics **71** (2006) T109.
5) M. Sato: Jpn. J. Appl. Phys. **44** (2005) 4490.
6) M. Sato: Jpn. J. Appl. Phys. **46** (2007) 4514.
7) M. Sato: Jpn. J. Appl. Phys. **47** (2008) 3931.
8) V. I. Levedev: USSR Comput. Math. Math. Phys. **4** (1964) 69.
9) V. Lisitsa and D. Vishnevskiy: Geophys. Prospect. **58** (2010) 619.
10) H. Bernth and C. Chapman: Geophysics **76** (2011) WA43.
11) P. Moczo, J. Kristek, and L. Halada: *The Finite Difference Method for Seismologists. An Introduction* (Comenius University, Bratislava, 2004) p. 9.
12) A. Taflove and S. C. Hagness: *Computational Electromagnetics* (Artech House, Boston, MA, 2005) 3rd ed.
13) T. Weiland: AEU-Int. J. Electron. Commun. **31** (1977) 116 [in German].
14) M. Clemens and T. Weiland: Prog. Electron. Res. **32** (2001) 65.
15) P. Fellinger, R. Marklein, K. J. Langenberg, and S. Klaholz: Wave Motion **21** (1995) 47.
16) U. S. Inan and R. A. Marshall: *Numerical Electromagnetics: The FD-TD Method* (Cambridge University Press, New York, 2011).
17) P. K. Chinta, K. Mayer, and K. J. Langenberg: AIP Conf. Proc. **1433** (2012) 487.
18) K. Hasegawa and T. Shimada: Jpn. J. Appl. Phys. **51** (2012) 07GB04.
19) J. Kristek, P. Moczo, and R. J. Archuleta: Stud. Geophys. Geod. **46** (2002) 355.

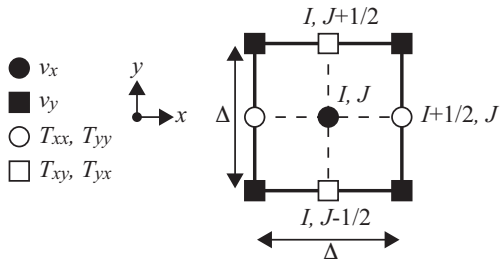


**Fig. 1.** Unit cell of the conventional staggered grids in two dimensions for P- and SV-waves propagation.

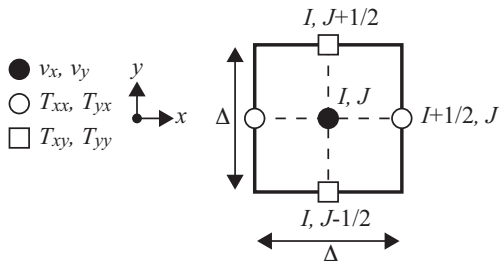


**Fig. 2.** Unit cell of the staggered grid using the collocated grid points of velocities (SGCV) in two dimensions for P- and SV-wave propagation.

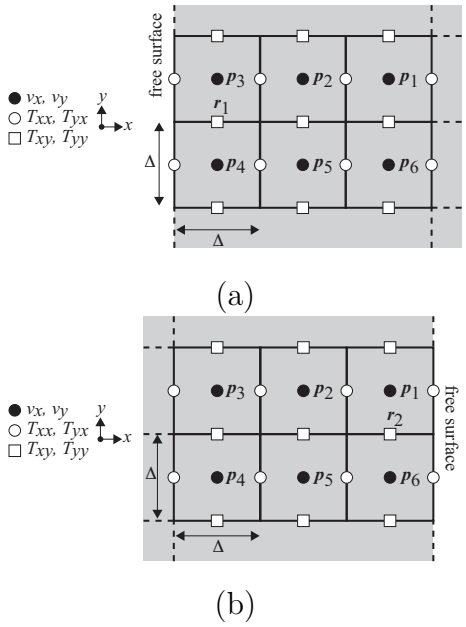


**Fig. 3.** Cells on free surfaces normal to the $x$-axis: (a) Free surface on the left side of an elastic body and (b) Free surface on the right side of an elastic body.

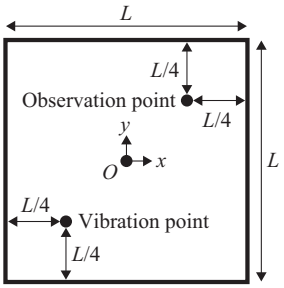


**Fig. 4.** Lamé mode resonator on an isotropic solid.

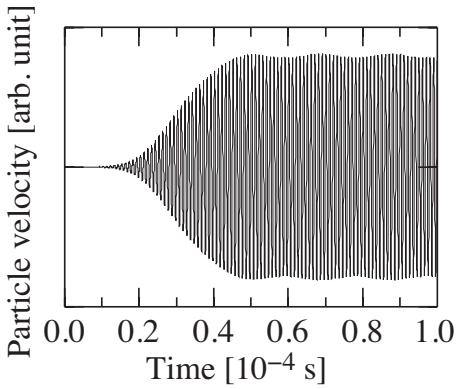


**Fig. 5.** Time response at the observation point.

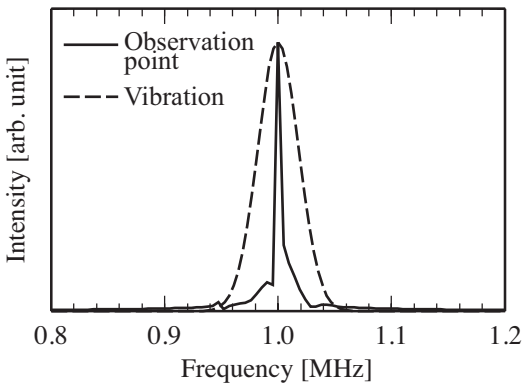


**Fig. 6.** Power spectra of $x$-components of particle velocities of the vibration and observation points with $L/\Delta = 2^6$, $N_s\Delta_t = 2^8 RLv_p \approx 52.25$ $\mu$s, $N_e\Delta_t = 2^{10}RL/v_p$, and the coefficients $C_{10}$ and $C_{01}$, computed using six adjoining grids.

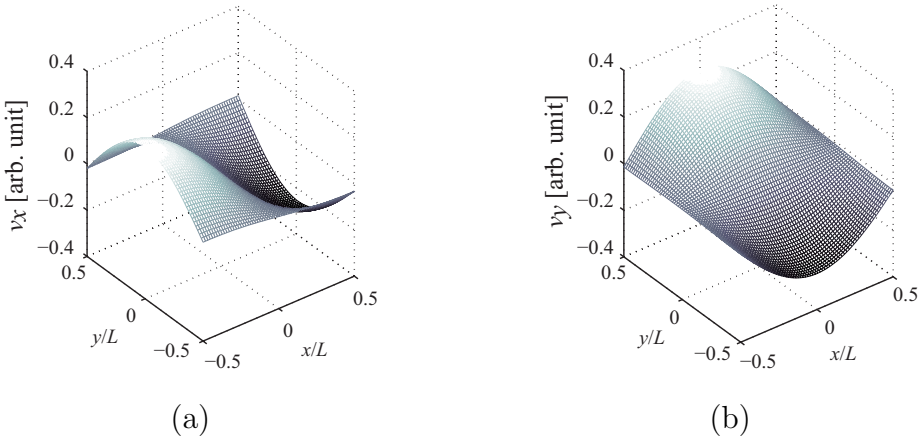


**Fig. 7.** Distributions of the particle velocity components (a) $v_x$ and (b) $v_y$ at $t = N_e\Delta_t$ for the same model as used in Fig. 6.

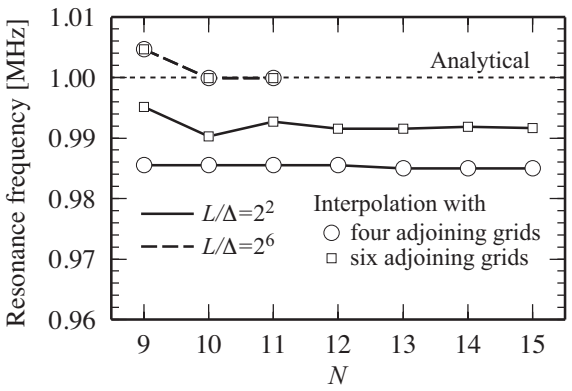


**Fig. 8.** Extracted resonance frequencies. The total number of time steps is given as $2^N$.